Electrical Pump-and-Probe Study of Spin Singlet-Triplet Relaxation in a Quantum Dot

S. Sasaki,[1,*] T. Fujisawa,[1,2] T. Hayashi,[1] and Y. Hirayama[1,3]

[1]*NTT Basic Research Laboratories, NTT Corporation, Atsugi-shi, Kanagawa 243-0198, Japan*
[2]*Tokyo Institute of Technology, 2-12-1 Ookayama, Meguro-ku, Tokyo 152-8551, Japan*
[3]*SORST-JST, 4-1-8 Honmachi, Kawaguchi, Saitama 331-0012, Japan*

(Received 9 February 2005; published 28 July 2005)

Spin relaxation from a triplet excited state to a singlet ground state in a semiconductor quantum dot is studied by employing an electrical pump-and-probe method. Spin relaxation occurs via cotunneling when the tunneling rate is relatively large, confirmed by a characteristic square dependence of the relaxation rate on the tunneling rate. When cotunneling is suppressed by reducing the tunneling rate, the intrinsic spin relaxation is dominated by spin-orbit interaction. We discuss a selection rule of the spin-orbit interaction based on the observed double-exponential decay of the triplet state.

DOI: 10.1103/PhysRevLett.95.056803 PACS numbers: 73.61.Ey, 73.23.Hk, 73.63.Kv

Electron spin in semiconductors has been a focus of research in the context of spintronics, in which spin is manipulated with spin-orbit coupling [1,2], and of quantum computation, in which spin carries a quantum information [3]. In contrast to two-dimensional electron gas (2DEG) with continuum density of states, electron spin in a quantum dot (QD) is basically free from elastic scattering, and the resulting long-lived spin states are favorable for spin-based applications. Indeed, relaxation times of more than 100 μs have been reported in QDs between Zeeman sublevels [4–6], as well as between a spin triplet and a singlet state [7,8]. These relaxation processes have been discussed in terms of either spin-orbit interaction or the cotunneling effect. In this Letter, we study spin relaxation from a triplet state to a singlet state in a lateral QD, in which all the relevant parameters can be controlled with the gate voltages. We observe smooth transition of the relaxation mechanism from the cotunneling regime to the spin-orbit regime by changing tunneling rates. The decay of the excited triplet state follows a single exponential curve in most conditions, but double-exponential behavior is observed at a particular magnetic field where the triplet state crosses another state. This might be related to the long-lived spin-entanglement state under strong spin-orbit interaction.

Figure 1(a) shows a scanning electron micrograph (SEM) image of our QD device. The $Al_xGa_{1-x}As$ 2DEG is constricted by combined dry-etching and surface Shottky gates. We use only the three gates on the right-hand side to form a single QD as shown by the white circle. All the measurements are performed in a dilution refrigerator at ~90 mK with magnetic field B applied perpendicularly to the 2DEG.

The dot used in this study has charging energy of $U \sim 2$ meV and electron number $N \sim 8$. When the magnetic field is not very small ($B > 0.4$ T), electron orbitals in a QD can be classified by the Landau level (LL) index, which they approach in the high field limit [9]. Many-body correction of direct and exchange Coulomb interactions induces spin and orbital transitions associated with different LLs in low magnetic field, but with the same LL in high magnetic field [10]. Figure 1(b) shows an observed dc current I through the dot as a function of the left gate voltage V_L and B. The two stripes show a pairwise motion

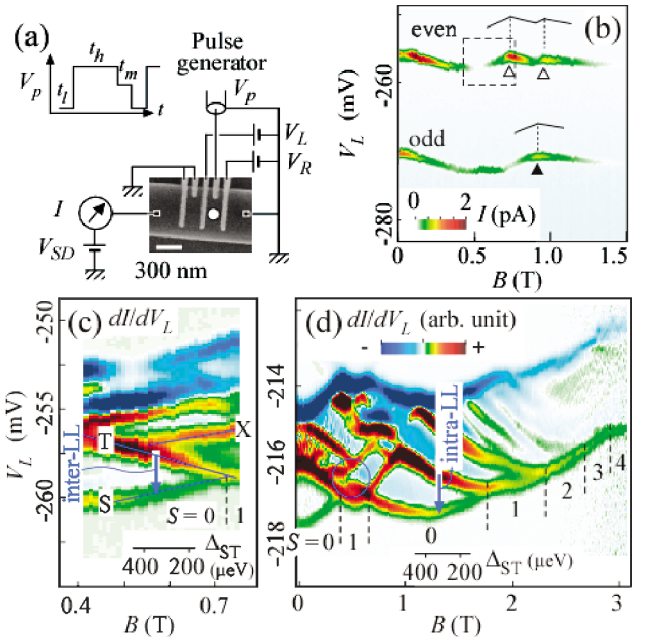

FIG. 1 (color). (a) SEM picture of the device together with a schematic of the measurement set-up. (b) dc current I as a function of V_L and B measured at $V_{sd} = 0.15$ mV in the first cooldown. I for the even N data is divided by 10. Evolution of the current peak is sketched around the transition fields (triangles). (c) dI/dV_L at $V_{sd} = 1.2$ mV taken at the dashed square region shown in (b). Δ_{ST} scale shows the region where the spin relaxation measurement is conducted. (d) dI/dV_L at $V_{sd} = 1.0$ mV measured in the second cooldown. The vertical dashed lines denote spin transitions of the ground state. A blue circle marks an anticrossing between two singlet states. Intensity for the high B data is enhanced by multiplying some smooth numerical function.

with B reflecting spin degeneracy. The lower stripe, corresponding to odd N, involves a level crossing (denoted by a solid triangle), associated with two orbitals in different LLs. The upper stripe for even N involves two spin transitions (open triangles) under Coulomb interactions. The ground state for even N is assigned to be spin triplet between the two transition fields, otherwise spin singlet state [10]. These spin states can be observed in the excitation spectrum of Fig. 1(c), in which the derivative of the current, dI/dV_L, with a large $V_{sd} = 1.2$ mV, is plotted as a function of V_L and B. Some excited states as well as the ground state that fall within the source-drain transport window are observed. We study spin relaxation from the triplet excited state to the singlet ground state (denoted by the arrow) separated by energy, Δ_{ST}. This relaxation involves orbital change between different LLs (inter-LL transition). Figure 1(d) is another excitation spectrum taken with the same device but in the second cooldown. In addition to the similar singlet-triplet transitions at $B \sim 0.5$ T, four spin-flip transitions are resolved at $B = 2$–3 T until the system enters a stable totally spin-polarized regime ($\nu = 1$), from which $N = 8$ is estimated [9]. We also study spin triplet-singlet relaxation (denoted by the arrow) that involves orbital change within the same LL (intra-LL transition). The measurement in the 1st (2nd) cooldown with relatively fast (slow) cooling speed resulted in moderate tunnel rates and spin transition fields suitable for studying spin relaxation involving inter- (intra-) LL transition, but both sets of data show similar characteristics.

An electrical pump-and-probe measurement is performed by applying two-step square pulses to the plunger gate [7]. First, the singlet and triplet states are emptied by lifting both states above the Fermi energy as shown in the inset to Fig. 2(a) (initialization). The duration of this initialization is t_l. Next, both states are pulled down below the Fermi energy as shown in the inset to Fig. 2(b). Then, only one electron can enter the dot because of the Coulomb blockade. This electron, if it populates the triplet state with a probability P, is allowed to relax to the singlet ground state while the pulse height is kept at this condition during the wait time, t_h. The three triplet sublevels with $S_Z = \pm 1, 0$ are presumably populated with an equal probability since the Zeeman splitting is negligibly small and the tunneling probability does not depend on S_Z. Finally, the pulse height is adjusted so that only the triplet state is within the transport window of 150 μeV defined by the Fermi energy of the left and right leads (readout). Then, the electron can contribute to the current only if it remains in the triplet state after t_h. This readout pulse width t_m is fixed to 500 ns. Actually, several electrons $[1/(1-P)]$ flow during this time for the unrelaxed case. Therefore, the average number of tunneling electrons per one pulse cycle n_t follows an exponential decay $n_t = \frac{P}{1-P} \times \exp(-t_h/\tau_s)$, from which the spin relaxation time τ_s can be determined [7].

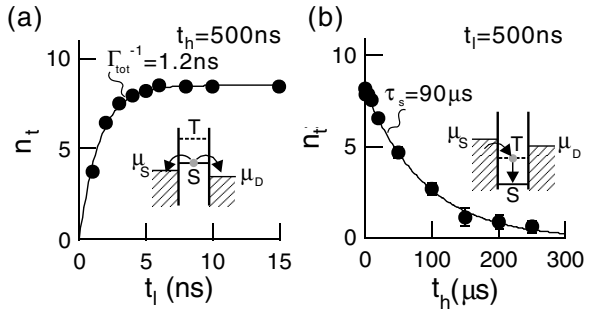

FIG. 2. (a) n_t as a function of the initialization time t_l with $\Delta_{ST} = 300$ μeV ($B = 0.6$ T in the first cooldown). The inset shows the energy diagram of the initialization process. (b) n_t as a function of the wait time, t_h. The inset shows the energy diagram of the relaxation process.

Figure 2(b) shows observed n_t as a function of t_h at $\Delta_{ST} = 300$ μeV. n_t shows a single exponential decay with $\tau_s = 90$ μs. The relatively large $n_t(t_h = 0) \simeq 8$, corresponding to $P \simeq 0.89$, comes from the fact that an injection into the triplet (singlet) state is more (less) effective because an electron is added to the outer (inner) orbital with a larger (smaller) tunneling rate in this magnetic field region [9].

We can also determine the total tunneling rate, $\Gamma_{tot}(= \Gamma_L + \Gamma_R)$ by changing the initialization pulse width, t_l. Here, Γ_L (Γ_R) is the tunneling rate for the left (right) barrier, which is changed by V_L (V_R). Figure 2(a) shows an example of such measurement. The rise time corresponds to the escape time from the singlet ground state through both tunneling barriers, and Γ_{tot} is estimated by fitting the data to the expression $n_t = \frac{P}{1-P}\{1 - \exp(-t_l\Gamma_{tot})\}$. Γ_{tot} is successfully changed between 1×10^8 and 3×10^9 s^{-1} by changing the gate voltages.

When Γ_{tot} is large, higher-order tunneling, or cotunneling, is quite effective in causing an exchange of electrons having opposite spins between the dot and the lead electrodes, resulting in a spin relaxation. According to the second-order perturbation theory, the cotunneling rate τ_{cot}^{-1} is approximately given by

$$\tau_{cot}^{-1} = \Delta_{ST}(\hbar\Gamma_{tot}^*)^2(\delta_-^{-1} + \delta_+^{-1})^2/h, \quad (1)$$

where δ_- and δ_+ are energies required to excite the N-electron triplet state to $N-1$- and $N+1$-electron virtual states, respectively [7]. Γ_{tot}^* is the effective tunneling rate for the cotunneling process from the triplet to the singlet state through either virtual state, while the experimentally obtained Γ_{tot} measures the tunneling rate from the singlet state to $N-1$-electron state. Figure 3(a) shows observed τ_s as a function of Γ_{tot} for representative conditions. The data points at large Γ_{tot} are almost parallel with the dotted line having a slope -2, i.e., $\tau_{cot}^{-1} = \alpha\Gamma_{tot}^2$, which is consistent with Eq. (1), assuming a linear relation $\Gamma_{tot}^* = \beta\Gamma_{tot}$. Figure 3(b) compares the observed Δ_{ST}

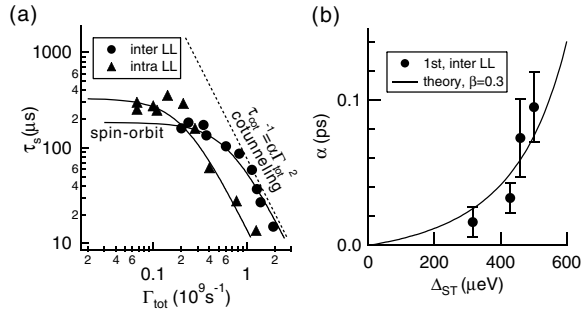

FIG. 3. (a) Log-log plot of τ_s as a function of Γ_{tot}. τ_s for inter-LL is measured at $B = 0.6$ T ($\Delta_{ST} = 300$ μeV) in the 1st cooldown, while that for intra-LL is measured at $B = 1.2$ T ($\Delta_{ST} = 380$ μeV) in the 2nd cooldown. The solid lines are fitted to the data. (b) The coefficient α for the cotunneling component as a function of Δ_{ST}. The curve is calculated with an effective tunneling rate, $\Gamma^*_{tot} = \beta\Gamma_{tot}$.

dependence of α with calculated $\alpha = \{h\Delta_{ST}(\delta_-^{-1} + \delta_+^{-1})^2\beta^2\}/4\pi^2$. We take $\delta_- = \delta_+ = (U/2 - \Delta_{ST})$ in the calculation, which approximates the experimental conditions. β of 0.3 gives a reasonable fit to the experimental results. Therefore, spin relaxation in the large Γ_{tot} regime can be well explained by the standard cotunneling theory.

It is seen in Fig. 3(a) that, when Γ_{tot} is reduced, τ_s increases and eventually saturates. In this regime, the cotunneling process is suppressed, and inelastic spin relaxation is dominated by phonon emission under the spin-orbit coupling effect rather than by coupling to nuclear spins, etc. [6,8,11]. The solid lines in Fig. 3(a) are the curves $(1/\tau_{so} + 1/\tau_{cot})^{-1}$ fitted to the data. Here, τ_{so} is the relaxation time due to the spin-orbit interaction, which is independent of Γ_{tot}.

Figure 4(b) shows the Δ_{ST} dependence of τ_s measured in the small Γ_{tot} regime where spin-orbit interaction is dominant. τ_s is almost constant in a wide Δ_{ST} regime (except at a dip around $\Delta_{ST} \sim 380$ μeV) and tends to increase when $\Delta_{ST} < 200$ μeV for both inter- and intra-LL data. This feature might have arisen from the phonon emission spectra in a QD in the presence of spin-orbit coupling. The phonon emission rate is maximized when the phonon wavelength is comparable to the dot size (phonon energy of 300 μeV for the dot size of 30 nm in the crystal growth direction) [7,12]. The similarity of the Δ_{ST} dependence of the inter- and intra-LL data supports this crude model. Longer τ_s is observed for the intra-LL case than for the inter-LL case in the whole Δ_{ST} region explored. This might reflect the different orbital quantum numbers involved in each case, which are relevant to the orbital effect on the phonon emission and spin-orbit interaction [13,14]. However, the precise mechanism is not clear yet.

Generally, in a one-electron system, the spin-up (down) state of one orbital is coupled with the spin-down (up) state of the other orbital when spin-orbit coupling is considered between the two orbitals [14]. This coupling gives rise to finite phonon emission probability between Zeeman sublevels. In the case of two-electron singlet/triplet states, singlet state ($|S\rangle$) is coupled with two of the triplet sublevels ($|T_+\rangle$ and $|T_-\rangle$) having $S_Z = \pm 1$, but not with the other sublevel ($|T_0\rangle$) having $S_Z = 0$ [11,15]. Therefore, relaxation from the triplet to the singlet state should have a selection rule in which the $|T_0\rangle$ state is still free from the spin-orbit relaxation mechanism as shown in Fig. 4(d). This simple argument applies when the singlet-triplet energies are so close to each other that coupling with other states is negligible. Unfortunately, our pump-and-probe technique is not available for the small Δ_{ST} regime because the minimum energy resolution is about 100 μeV. When another singlet excited state is involved, however, clear selectivity may appear in the vicinity of the level crossing between the triplet and the singlet excited states.

Actually, as shown in Fig. 1(c), we do see a level crossing with an unknown state (X) at about $B \simeq 0.52$ T ($\Delta_{ST} \simeq 400$ μeV) that could be a singlet state. When the dot potential has no rotational symmetry, large anticrossing is expected between the *same* spin states [16]. Typical anticrossing energy between the same spin states in our noncircular dot device is about 150 μeV [for instance, marked by the circle in Fig. 1(d)]. The unresolved anticrossing

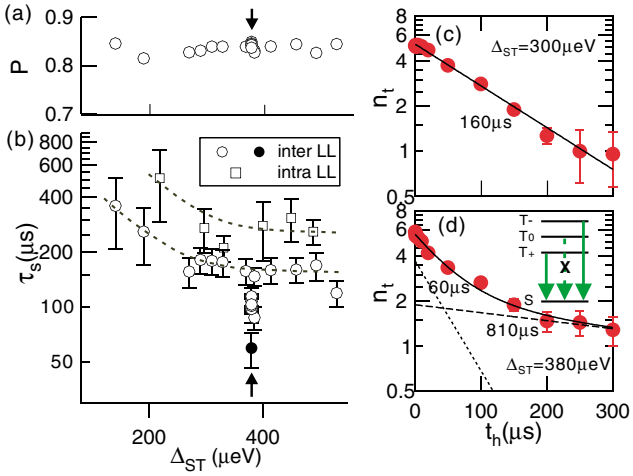

FIG. 4 (color online). (a) Δ_{ST} dependence of the excitation probability P for the inter-LL relaxation (1st cooldown). (b) Δ_{ST} dependence of the τ_s for the inter- and intra-LL relaxations. Data with open symbols are obtained by fitting a single exponential function, while the solid circle represents the fast component of the double-exponential function. The dotted lines are guides for the eye. (c) A logarithmic plot of n_t vs t_h with $\Gamma_{tot} = 2.0 \times 10^8$ s^{-1} at $\Delta_{ST} = 300$ μeV ($B = 0.6$ T). The solid line is an exponential function fitted to the data. (d) A logarithmic plot of n_t vs t_h with $\Gamma_{tot} = 2.7 \times 10^8$ s^{-1} at $\Delta_{ST} = 380$ μeV ($B = 0.55$ T). The solid line is a double-exponential function fitted to the data. The dotted and dashed lines are the fast and slow components, respectively. The inset schematically shows allowed and forbidden transitions from the triplet sublevels to the singlet state.

between T and X states (<100 μeV) implies that X is a singlet state. As shown by the arrow in Fig. 4(b), a sharp dip in τ_s is observed at $\Delta_{ST} \simeq 380$ μeV close to the X-T crossing point. The width of the dip is as narrow as about 20 μeV in Δ_{ST} ($\sim$10 mT in B) [17]. The dip could be attributed to strong spin-orbit coupling around the crossing point, resulting in the short relaxation time, as theoretically predicted in Ref. [14]. It should be noted that the decay of the pulse-induced current shows a nonsingle exponential behavior around the dip as shown in Fig. 4(d), while single exponential decay is always observed at other conditions, e.g., at $\Delta_{ST} = 300$ μeV shown in Fig. 4(c). The decay characteristic in Fig. 4(d) can be very well fitted with a double-exponential function (the solid line); $C_1 \exp(-t_h/\tau_{so}) + C_2 \exp(-t_h/\tau_{cot})$. Here, C_1, C_2, and τ_{so} are fitting parameters, and τ_{cot} is an input parameter ($=810$ μs) determined by extrapolating the Γ_{tot} dependence of τ_s in the cotunneling regime to the present value of Γ_{tot}. The fast component of the double-exponential decay can be assigned to the relaxation from $|T_+\rangle$ and $|T_-\rangle$ via spin-orbit coupling, while the slow component to the relaxation from $|T_0\rangle$ via higher-order spin-orbit coupling or the remaining cotunneling contribution. We find that the obtained ratio of C_1/C_2 is 2.0 and τ_{so} is 60 μs. The ratio C_1/C_2 obtained at slightly different Γ_{tot} ranges between 1.6 and 2.0. These values of C_1/C_2 are close to 2, which is expected for an equal population of the three triplet sublevels.

The above observations agree well with the selection rule for spin-orbit coupling that is enhanced in the vicinity of the X-T crossing. However, we cannot safely rule out other possibilities like populating an X state in addition to the triplet state of interest. Indeed, a very small increase ($\simeq 1\%$) in the excitation probability P is noted at around $B = 0.55$ T as shown by the arrow in Fig. 4(a), which could be due to injection into the X state. However, this effect is too small to explain the observed double-exponential behavior. Another possibility might be coupling to nuclear spins, which often appears at the level coincidence of different spin states [18].

In summary, we have studied spin relaxation dynamics from the triplet excited state to the singlet ground state in a lateral QD. The dominant spin relaxation mechanism is cotunneling at a large tunneling rate, and it changes to spin-orbit interaction when cotunneling is suppressed. The observed double-exponential decay characteristic could reflect the selection rule for the singlet-triplet transition mediated by spin-orbit interaction. Further investigation is required to prove this is the case.

We can think of an "entanglement generator" using this selection rule: The singlet ground state $|S\rangle = |\uparrow\rangle_a|\downarrow\rangle_a$ holds a spin pair in an orbital a, while the triplet state contains nonentangled states $|T_+\rangle = |\uparrow\rangle_a|\uparrow\rangle_b$ and $|T_-\rangle = |\downarrow\rangle_a|\downarrow\rangle_b$, and entangled state $|T_0\rangle = \frac{1}{\sqrt{2}}(|\uparrow\rangle_a|\downarrow\rangle_b + |\downarrow\rangle_a|\uparrow\rangle_b)$, with an electron in each of the orbitals a and b. At a proper waiting time after the electron injection [e.g., $t_h = 300$ μs in the case of Fig. 4(d)], the system is left in the entangled triplet state $|T_0\rangle$ with a probability of 18% [$n_t(t_h = 300\ \mu s) \times (1 - P)$], or otherwise in the singlet ground state $|S\rangle$. Our pulse measurement is based on the extraction of an electron from the unrelaxed $|T_0\rangle$ state (the outer orbital with the high probability P), and thus this scheme can be used to generate or analyze an entangled spin pair by detecting the extracted electron with a sensitive electrometer [5,8].

The authors acknowledge valuable discussions with Dr. A. V. Khaetskii and Y. Tokura. The work is financially supported by SORST-JST and Grant-in-Aid for Scientific Research from the Japan Society for the Promotion of Science.

*Electronic address: satoshi@nttbrl.jp

[1] *Semiconductor Spintronics and Quantum Computing*, edited by D. D. Awschalom, D. Loss, and N. Samarth (Springer, New York, 2002).
[2] S. Datta and B. Das, Appl. Phys. Lett. **56**, 665 (1990).
[3] D. Loss and D. P. DiVincenzo, Phys. Rev. A **57**, 120 (1998).
[4] R. Hanson *et al.*, Phys. Rev. Lett. **91**, 196802 (2003).
[5] J. M. Elzerman *et al.*, Nature (London) **430**, 431 (2004).
[6] M. Kroutvar *et al.*, Nature (London) **432**, 81 (2004).
[7] T. Fujisawa *et al.*, Nature (London) **419**, 278 (2002); T. Fujisawa *et al.*, J. Phys. Condens. Matter **15**, R1395 (2003).
[8] R. Hanson *et al.*, Phys. Rev. Lett. **94**, 196802 (2005).
[9] M. Ciorga *et al.*, Phys. Rev. B **61**, R16315 (2000); A. S. Sachrajda *et al.*, Physica E (Amsterdam) **10**, 493 (2001); M. Ciorga *et al.*, Physica E (Amsterdam) **11**, 35 (2001).
[10] S. Tarucha *et al.*, Phys. Rev. Lett. **84**, 2485 (2000).
[11] A. V. Khaetskii and Y. V. Nazarov, Phys. Rev. B **61**, 12 639 (2000).
[12] U. Bockelmann and G. Bastard, Phys. Rev. B **42**, 8947 (1990).
[13] C. F. Destefani *et al.*, Phys. Rev. B **70**, 205315 (2004).
[14] D. V. Bulaev and D. Loss, Phys. Rev. B **71**, 205324 (2005).
[15] S. Dickmann and P. Hawrylak, J. Supercond. **16**, 387 (2003).
[16] P. S. Drouvelis *et al.*, J. Phys. Condens. Matter **16**, 3633 (2004); Y. Tokura *et al.*, Physica B (Amsterdam) **298**, 260 (2001); P. A. Maksym, Physica B (Amsterdam) **249**, 233 (1998).
[17] Because of the narrow feature, the dip was discovered only in the 1st cooldown, but reproduced well during the same cooldown.
[18] K. Ono and S. Tarucha, Phys. Rev. Lett. **92**, 256803 (2004).